Supporting information

Biomass Zein Improved GF Separator for Dendrite-Free Aqueous Zinc-Ion Batteries

Bozhong Cao[a#], Qian Qu[a#], Bingchun Jiang[a], Tianyu Zou[a], Shubing Zhen[a], Peiwen Wang[a], Kairui Li[a], Jincheng Zhang[a], Hui Guo[a], Tong Zhang[a,b*]

[a.] *College of Mechanical and Electrical Engineering, Guangdong University of Science and Technology, Dongguan 523000, China*

[b.] *Faculty of Digital Science and Technology, Macau Millennium College, 999078, China*

# These authors contributed to the work equally and should be regarded as co-first authors.

* Corresponding authors.

Experimental Section

Chemicals and materials.

All reagents and materials used in this study were obtained commercially without further purification. Zinc sulfate heptahydrate ($ZnSO_4 \cdot 7H_2O$, purity 99%), manganese sulfate monohydrate ($MnSO_4 \cdot H_2O$, purity 99%), Lithium bromide (LiBr, purity 99%), anhydrous ethanol (purity 99.5%), and Zein (from Corn) were purchased from Aladdin Reagent. Zn foil, Cu foil and Ti foil were purchased from Qingyuan Metal Materials. Glass fiber separator was purchased from Whatman.

Preparation of zein and zein/LiBr solutions.

A certain amount of zein was first dissolved in 80 wt% ethanol-water solution and stirred for 15 min at room temperature to obtain 0.08 g/mL of zein solution. Different amount of LiBr (0.02 g/mL, 0.04 g/mL, 0.06 g/mL) was added to the zein solution and stirred at 80 °C for 30 min, which was left to room temperature to obtain the zein/LiBr solution.

Preparation of Z-GF and ZLB-GF separator.

The glass fiber separator was immersed in the above zein solution, then treated with

ultrasound. Subsequently, ethanol and water were removed from the Z-GF separator by drying at 65 °C. ZLB-GF separator was also obtained by this method, only replace the zein solution with zein/LiBr solution

Preparation of the electrolytes.

The 2M $ZnSO_4$ electrolyte was prepared by dissolving zinc sulfate heptahydrate in deionized water.

Preparation of MnO_2 electrode.

MnO_2, Super P and PVDF were combined in a mass ratio of 7:2:1. To achieve a homogeneous slurry, an appropriate amount of N-methylpyrrolidone (NMP) solvent was added. This slurry was then coated onto a titanium foil using a 100 μm squeegee. The coating was then dried at 70°C.

Characterizations.

Surface morphology and corresponding elemental analysis were obtained using a Tescan Mira scanning electron microscope (SEM). X-ray diffraction (XRD) patterns were collected using a Rigaku SmartLab SE with Cu Kα (α = 1.5406 Å) as the radiation source. Fourier transform infrared (FTIR) spectroscopy was performed using a Thermo Scientific iN10 instrument. X-ray photoelectron spectroscopy (XPS) was conducted using a Thermo Scientific Kalpha spectrometer. Thermogravimetric(TG) was conducted using a Netzsch STA 449 F5. the tensile stress-strain curves of the separators were obtained using a tensile testing machine (CMT6103) at a cross-head speed of 1 mm/min. Laser scanning microscope images were obtained by 3D measuring laser microscope (Keyence VK-X1000).

Electrochemical Measurements.

The electrochemical measurements were conducted using symmetric/asymmetric/full cells

by assembling with GF or ZLB-GF into 2032-type coin cells at room temperature. Galvanostatic charge/discharge (GCD) cycling tests were carried out on the LAND CT3002A battery-testing system. Electrochemical impedance spectroscopy (EIS), chronoamperometry (CA), linear sweep voltammetry (LSV) and cyclic voltammetry (CV) measurements of the cells were recorded on an electrochemical workstation (CHI604E, China).

DFT calculation.

The binding energy of the configuration (Ebind) was calculated by the following equation.

$$E_{bind} = E_{AB}\text{-}(E_A + E_B)$$

In the above equation, E, Es, and Eas represent the energies of A (Zn^{2+}), B (single polymer), and the complex energy, respectively. A negative value for Ebind indicates an exothermic reaction, with a higher negative value indicating a stronger interaction. This stronger interaction corresponds to a greater release of heat and a more stable product.

Finite element modelling.

In the simplified model, the bare separator was built as a sieve plate with a thickness of 8.0 μm, which was composed of rectangular channels with an aperture of 1.0 μm and a hole spacing of 2.0 μm. Using a 0.05 μm film under the pristine separator to represent the coated zein. The cathodic potential was set as 150 mV, which was in line with the experimentally observed voltage hysteresis, while the prototype point was fixed at 0 V. The electrical conductivity of anode/cathode, GF separator and zein was 1.67×10^{7}, 1×10^{-7} and 1×10^{-16} $S\cdot m^{-1}$, respectively. The ionic conductivity of 2 M $ZnSO_4$ electrolyte was 5 $S\cdot m^{-1}$.

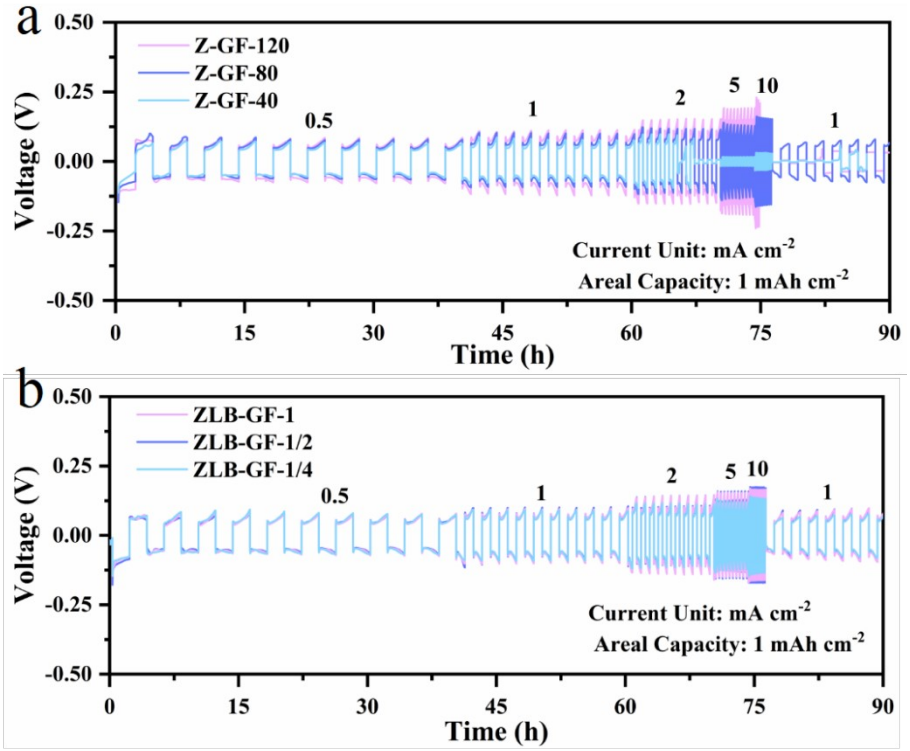

Figure S1. The rate performances of Z-GF-x(a) and ZLB-GF-y(b) separators at various current densities with a fixed areal capacity of 1 mAh·cm^{-2}.

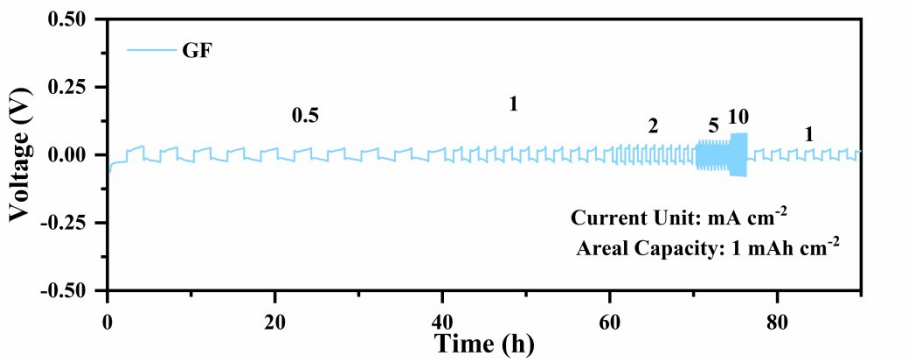

72

73 **Figure S2.** The rate performances of GF separator at various current densities with a fixed

74 areal capacity of 1 mAh·cm^{-2}.

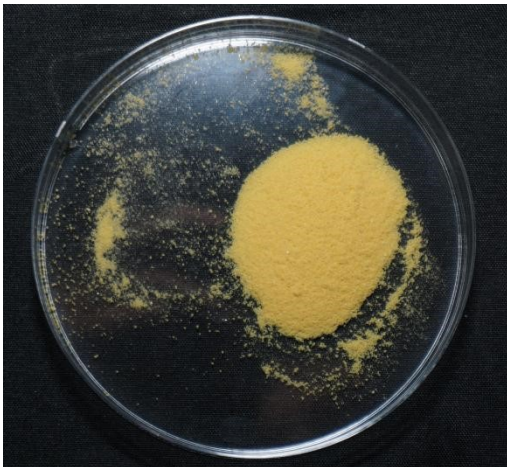

Figure S3. The picture of zein powder.

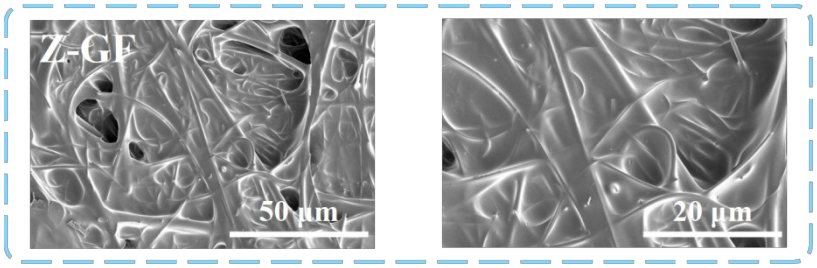

Figure S4. SEM images of Z-GF separator.

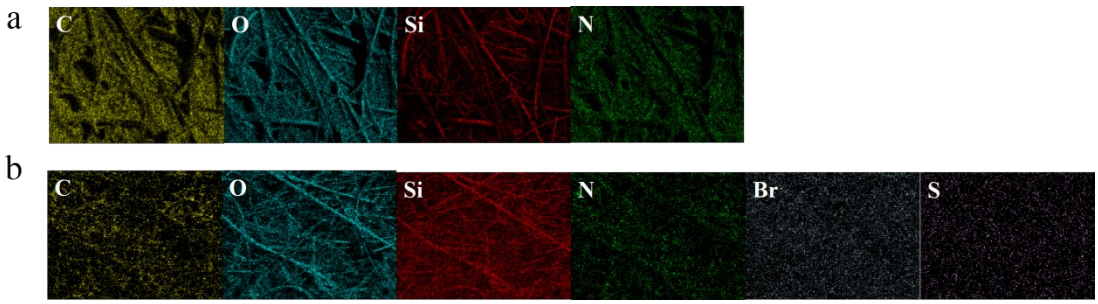

Figure S5. EDS mapping of (a) Z-GF and (b) ZLB-GF separator.

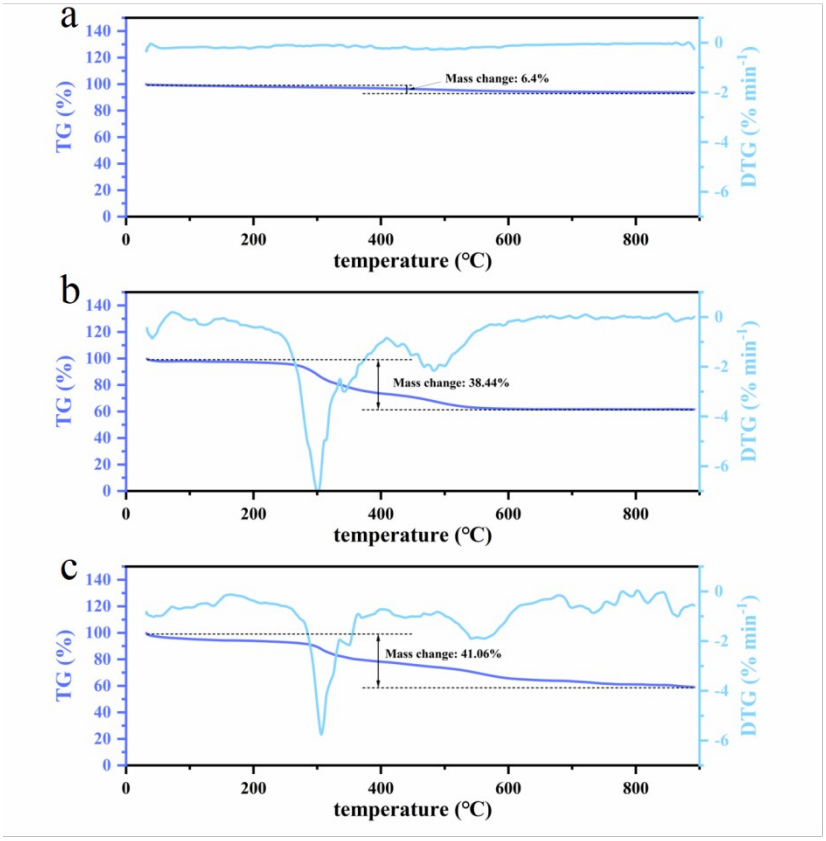

Figure S6. TG-DTA curves of GF (a), Z-GF(b) and ZLB-GF(c) separators.

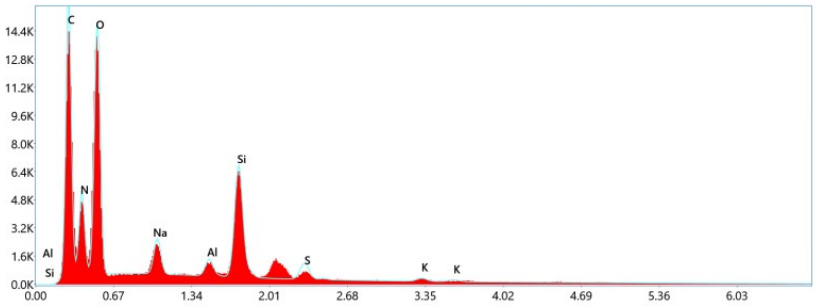

Figure S7. Elemental mapping result of the Z-GF separator.

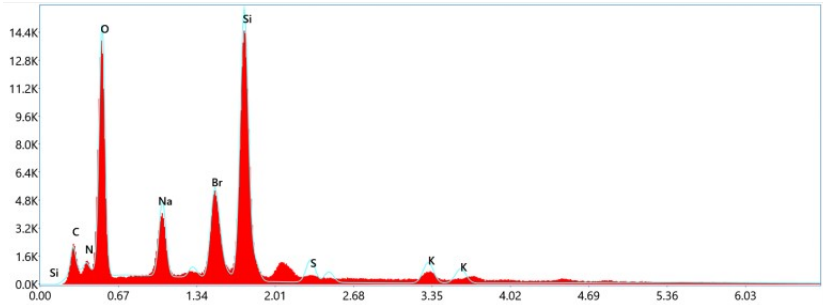

Figure S8. Elemental mapping result of the ZLB-GF separator.

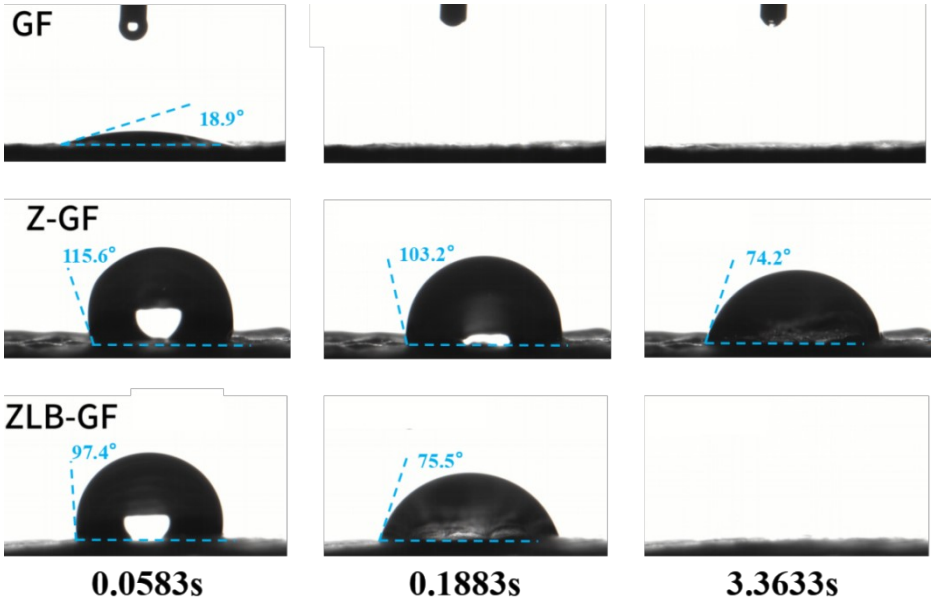

Figure S9. Contact angles of GF, Z-GF and ZLB-GF separators.

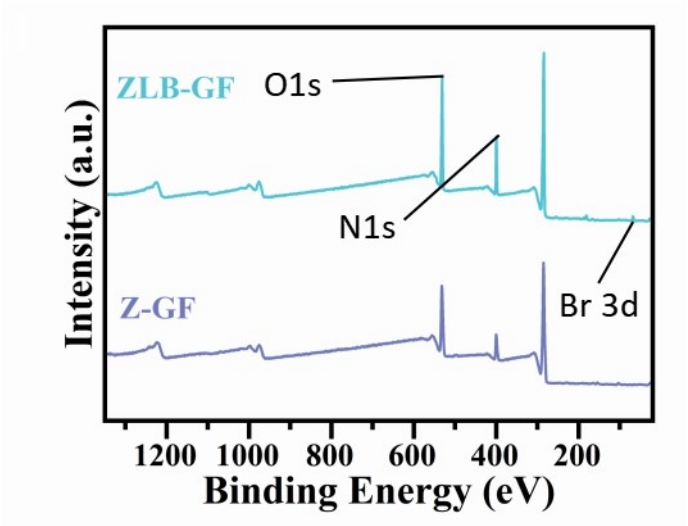

Figure S10. XPS spectra of Z-GF and ZLB-GF separators.

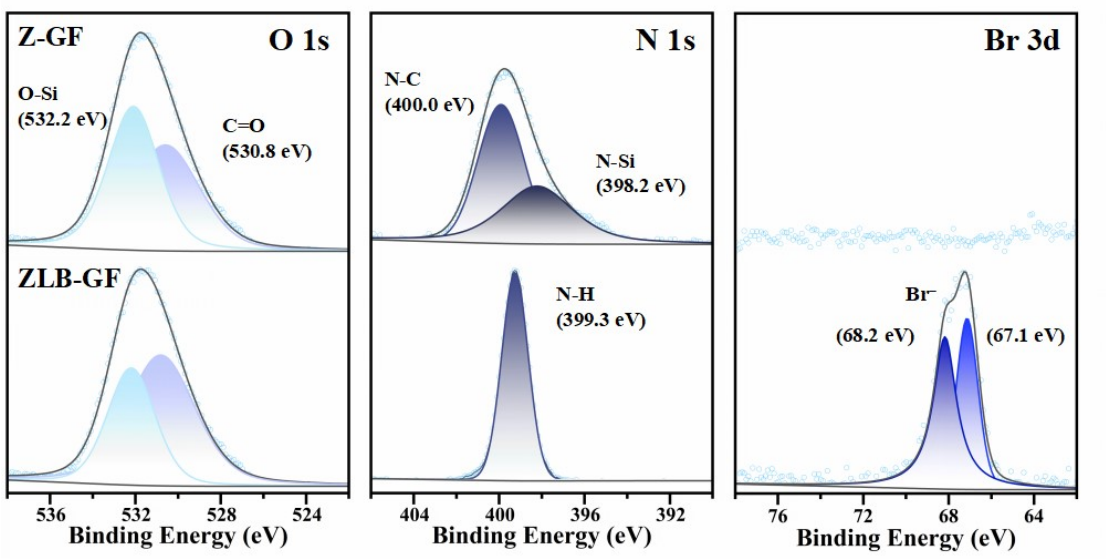

Figure S11. High-resolution O 1s,N 1s,Br 3d XPS spectra of Z-GF and ZLB-GF separators.

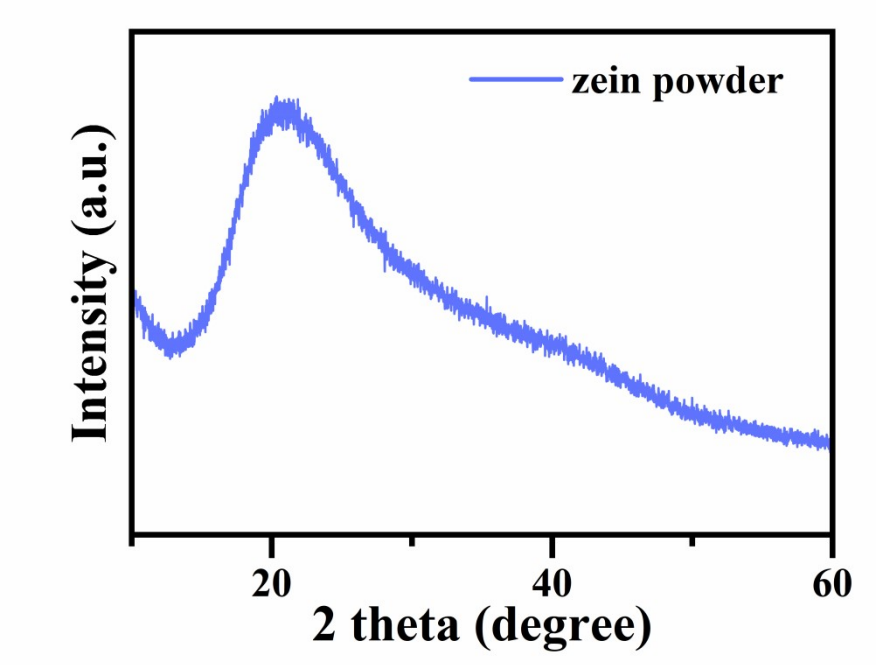

Figure S12. XRD spectra of zein powder.

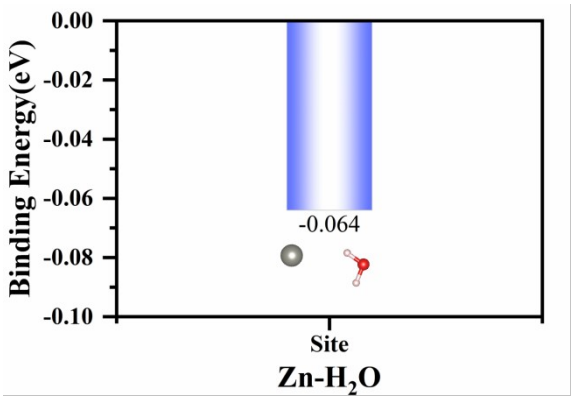

Figure S13. Binding energy between Zn^{2+} and H_2O molecule.

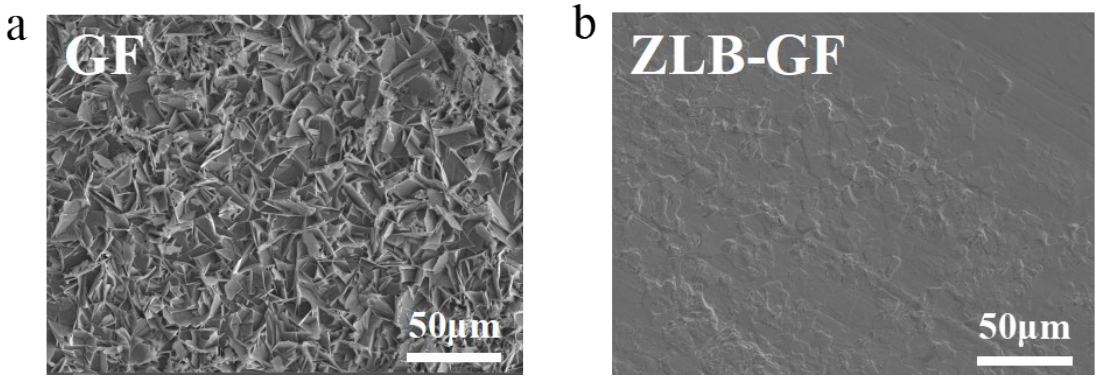

Figure S14. SEM images of zinc anode with (a) GF and (b) ZLB-GF resting for seven days.

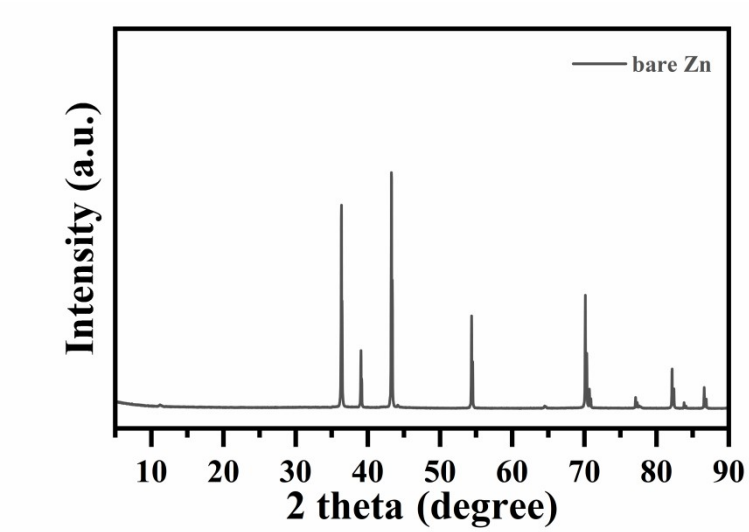

Figure S15. XRD spectra of bare Zn.

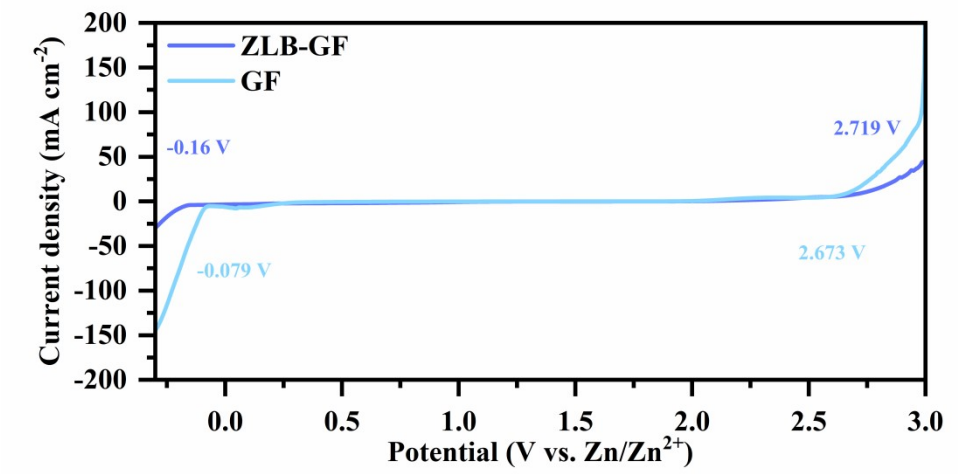

Figure S16. Electrochemical windows with GF and ZLB-GF separator obtained by LSV.

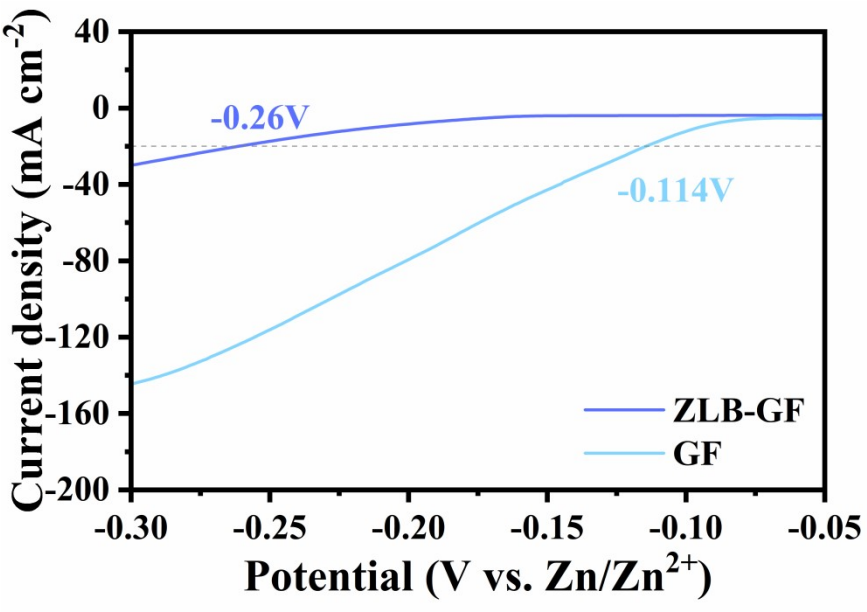

Figure S17. HER curves of $ZnSO_4$ electrolytes with GF and ZLB-GF.

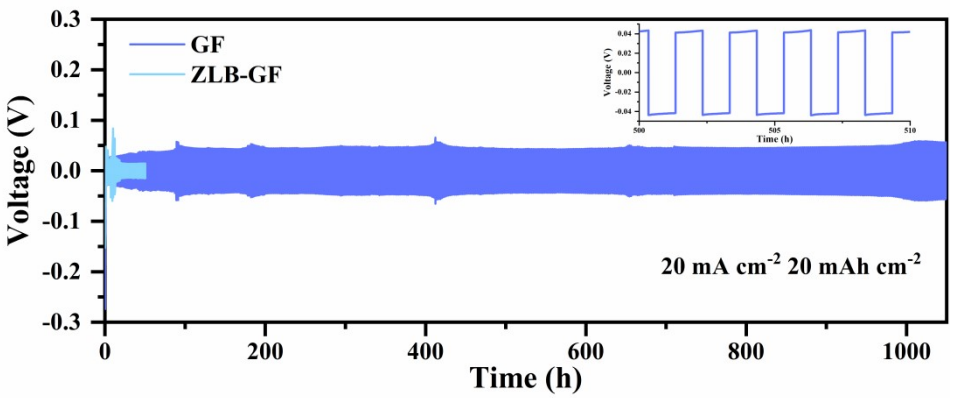

Figure S18. Cycling performance of Zn//Zn symmetric cells with GF and ZLB-GF separators.

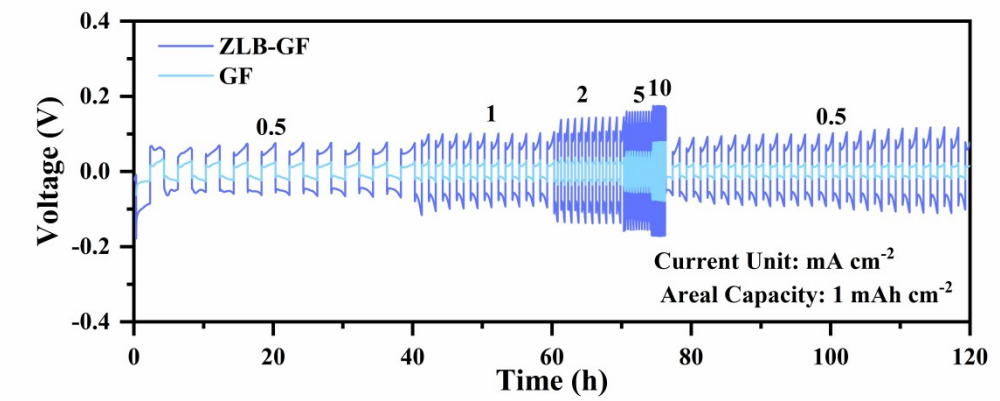

Figure S19. The rate performance of GF and ZLB-GF separators at various current densities with a fixed areal capacity of 1 mAh cm^{-2}.

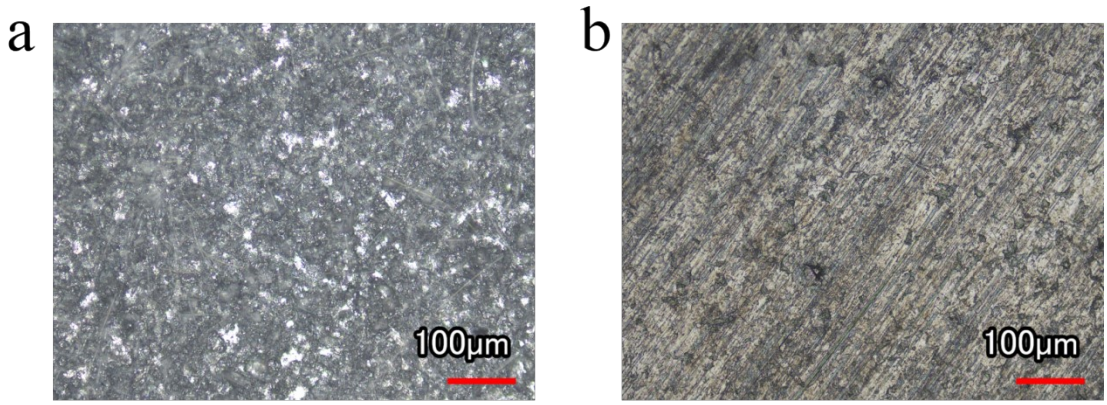

Figure S20. Optical micrographs of zinc anode after 100h of cycling using (a) GF and (b) ZLB-GF separators.

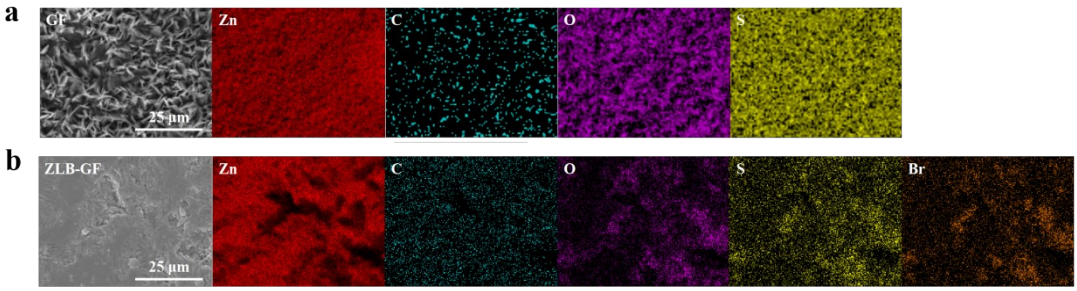

Figure S21. EDS mapping of zinc anode after 100h of cycling using (a) GF and (b) ZLB-GF separators.

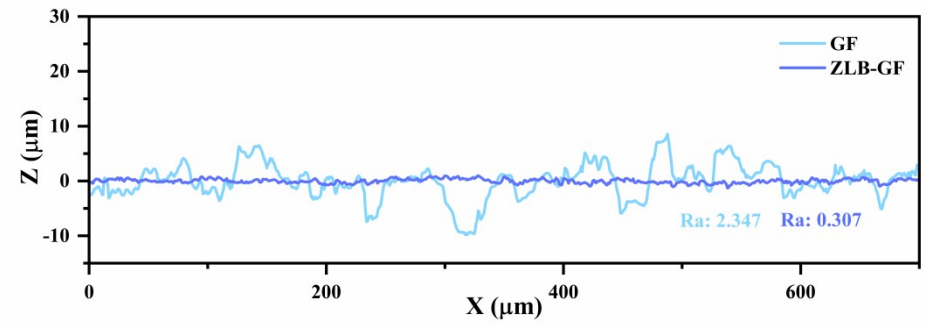

Figure S22. Surface roughness curves of zinc anode after 100h of cycling using GF and ZLB-GF separators.

Figure S23. Electronic snapshots of the separators after 100h of cycling using GF and ZLB-GF separators.

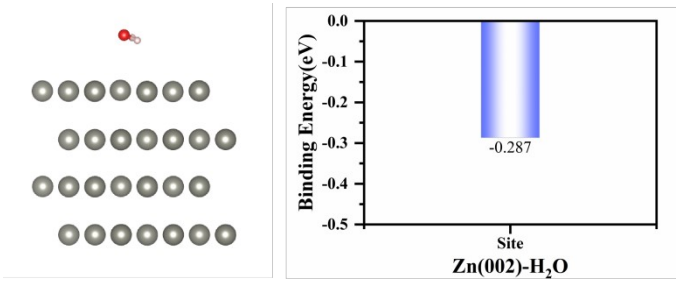

Figure S24. Binding energy between Zn and H_2O molecule.

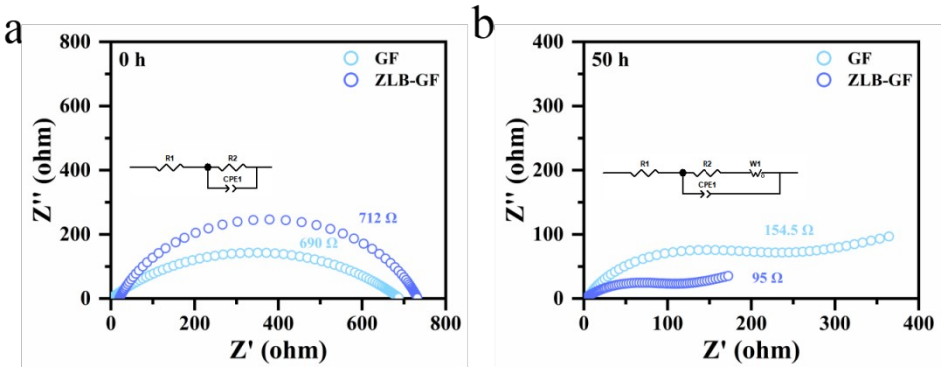

Figure S25. Nyquist plots of Zn//Zn symmetric cells using GF and ZLB-GF separators before (a) and after cycling (b).

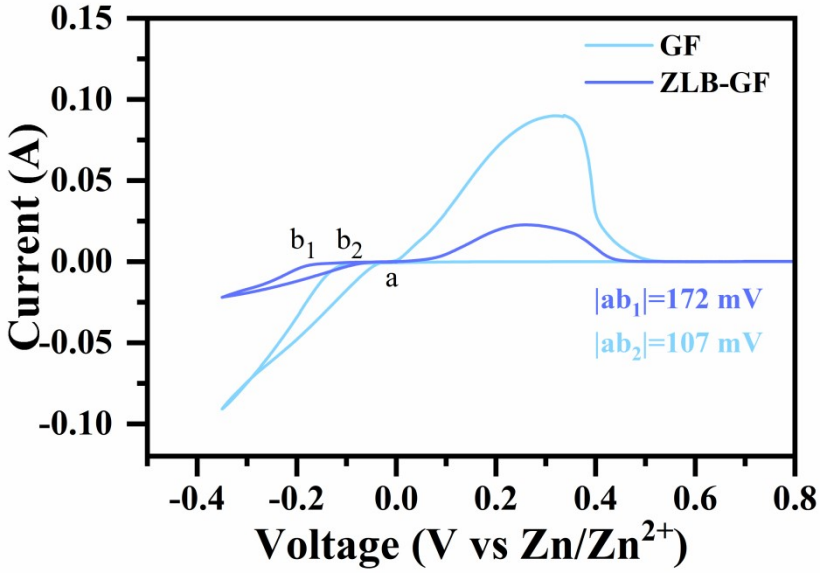

Figure S26. CV curves of Zn//Cu cells with GF and ZLB-GF separator.

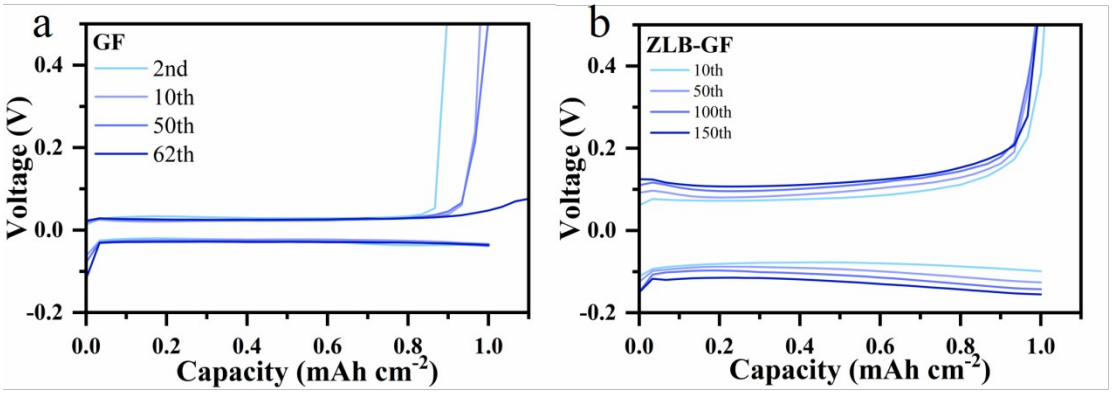

Figure S27. The GCD curves of Zn//Ti cells with (a) GF and (b) ZLB-GF separator.

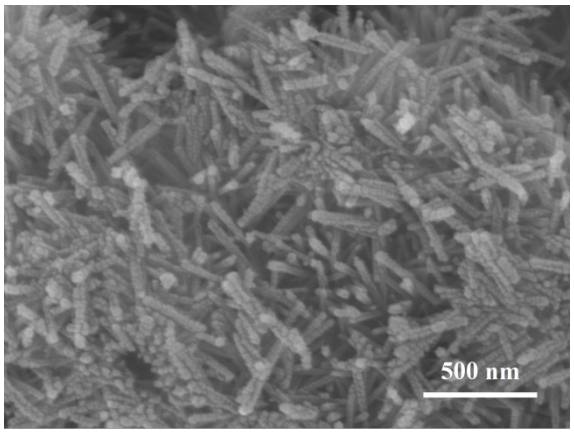

Figure S28. SEM image of MnO_2.

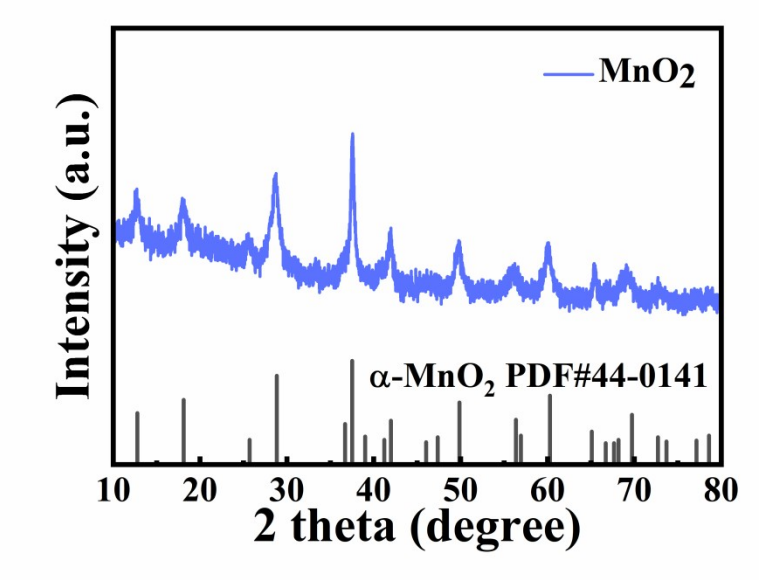

Figure S29. XRD pattern of MnO_2.

Table S1. Element Signal of Z-GF and ZLB-GF separator.

Element	Weight %	
	Z-GF	ZLB-GF
C	55.2	23.1
N	17.2	2.1
O	23.1	37.2
Si	2.9	22.7
S	1.6	3.0
Br	——	11.9

Table S2. Element Signal of zinc anode after 100h of cycling using GF and ZLB-GF separators.

Element	Weight %	
	GF	ZLB-GF
C	6.5	13.2
O	25.9	7.9
S	7.1	1.1
Zn	60.5	75.7
Br	——	2.1

Table S3. Comparison of the electrochemical performances of ZLB-GF separator with recently reported GF separator modification.

Functionalized Separator	Current density ($mA \cdot cm^{-2}$)	Capacity ($mAh \cdot cm^{-2}$)	Life (h)	Ref.
Modification zien	10	10	3100	This work
Cellulose paper	5	5	400	[1]
Ti_3C_2Tx MXene	1	1	1180	[2]
MXene@NiO modified separator	10	10	500	[3]
Vertical graphene	10	1	600	[4]
N-doped carbon	1	1	1100	[5]
$BaTiO_3$	10	2.5	1600	[6]
g-C_3N_4 coated separator	3	1	600	[7]
MOF UiO-66	2	1	1600	[8]
Sulfonic cellulose@graphene	10	10	1400	[9]

References

1. Z. Yang, W. Li, Q. Zhang, C. Xie, H. Ji, Y. Tang, Y. Li and H. Wang, *Materials Today Energy*, 2022, **28**, 101076.
2. Y. Su, B. Liu, Q. Zhang, J. Peng, C. Wei, S. Li, W. Li, Z. Xue, X. Yang and J. Sun, *Advanced Functional Materials*, 2022, **32**.
3. Y. An, Y. Tian, Q. Man, H. Shen, C. Liu, Y. Qian, S. Xiong, J. Feng and Y. Qian, *ACS Nano*, 2022, **16**, 6755-6770.
4. C. Li, Z. Sun, T. Yang, L. Yu, N. Wei, Z. Tian, J. Cai, J. Lv, Y. Shao, M. H. Rümmeli, J. Sun and Z. Liu, *Advanced Materials*, 2020, **32**, 2003425.
5. X. Yang, W. Li, J. Lv, G. Sun, Z. Shi, Y. Su, X. Lian, Y. Shao, A. Zhi, X. Tian, X. Bai, Z. Liu and J. Sun, *Nano Research*, 2022, **15**, 9785-9791.
6. Y. Liang, D. Ma, N. Zhao, Y. Wang, M. Yang, J. Ruan, G. Yang, H. Mi, C. He and P. Zhang, *Advanced Functional Materials*, 2022, **32**, 2112936.
7. L. Wu, Y. Zhang, P. Shang, Y. Dong and Z.-S. Wu, *Journal of Materials Chemistry A*, 2021, **9**, 27408-27414.
8. Y. Song, P. Ruan, C. Mao, Y. Chang, L. Wang, L. Dai, P. Zhou, B. Lu, J. Zhou and Z. He, *Nano-Micro Letters*, 2022, **14**.
9. X. Zhang, J. Li, K. Qi, Y. Yang, D. Liu, T. Wang, S. Liang, B. Lu, Y. Zhu and J. Zhou, *Adv Mater*, 2022, **34**, e2205175.